Central difference solutions of the kinematic model of settling of polydisperse suspensions and three-dimensional particle-scale simulations

R. Bürger
Institute of Mathematics A, University of Stuttgart, Pfaffenwaldring 57, 70569 Stuttgart, Germany, (buerger@mathematik.uni-stuttgart.de)

K.-K. Fjelde
RF-Rogaland Research, Thormøhlensgt. 55, N-5008 Bergen, Norway, (kjell-kaare.fjelde@rf.no)

K. Höfler
Institute for Computer Applications 1, University of Stuttgart, Pfaffenwaldring 27, 70569 Stuttgart, Germany, (kai@ica1.uni-stuttgart.de)

K. Hvistendahl Karlsen
(i) Department of Mathematics, University of Bergen, Johs. Brunsgt. 12, N-5008 Bergen, Norway, (kennethk@mi.uib.no)
(ii) RF-Rogaland Research, Thormøhlensgt. 55, N-5008 Bergen, Norway

Abstract. The extension of Kynch's kinematic theory of sedimentation of monodisperse suspensions to polydisperse mixtures leads to a nonlinear system of conservation laws for the volume fractions of each species. In this paper, we show that a second order central (Riemann solver free) scheme for the solution of systems of conservation laws can be employed as an efficient tool for the simulation of the settling and the separation of polydisperse suspensions. This is demonstrated by comparison with a published experiment of settling of a bidisperse suspension. In addition, we compare the prediction of the one-dimensional kinematic sedimentation model with a three-dimensional particle-scale simulation.

Keywords: Sedimentation, polydisperse suspension, system of conservation laws, central difference scheme, particle-scale simulation.

1. Introduction

Mathematical models for the settling of suspensions are of great theoretical and practical interest in numerous applications such as mineral processing [1], wastewater treatment [2] and blood centrifugation [3]. A well-known theory of one-dimensional sedimentation of ideal suspensions [4] is due to Kynch [5]. The essential assumption of this kinematic theory is that the solid-fluid relative velocity, or slip velocity, is a given function of the local volumetric solids concentration. The local solids mass balance then turns into a scalar conservation law. While Kynch's model and its extension to flocculated monodisperse suspensions are well understood now and have been validated for numerous real materials (see [1] for details), most implications of kinematic models for polydisperse suspensions (with particles differing in size or density) still remain to be explored. Exact entropy weak solutions even to the apparently simple problem of settling of a bidisperse, initially homogeneous suspension have not yet been determined, due to the nonlinear character of the system of two first-order partial differential equations involved. However, as we show here, modern entropy-satisfying shock capturing numerical schemes can be successfully employed to solve this problem numerically.

Although there is a large list of authors who have proposed extensions of Kynch's theory to the polydisperse case (see [6] for an overview), only few of them have embedded their equations into the appropriate mathematical framework of nonlinear systems of conservation laws [7, 8]. The essential property of solutions of these systems is the formation of discontinuities, which appear here in the concentrations of the different particle species. The presence of discontinuities requires the concept of weak solutions, which are not unique such that an additional selection principle or entropy condition is necessary to determine the physically relevant weak solution, the *entropy weak solution*. Discontinuities which are part of entropy weak solutions are called *shocks*.

Consequently, it is a desirable property of any numerical scheme suitable for the solution of the kinematic model of sedimentation of polydisperse suspensions to approximate the entropy weak solution, and to detect shocks automatically. Such schemes, which will produce accurate approximations to discontinuous solutions without explicitly using jump conditions and shock tracking techniques, are called *shock-capturing*. The last three decades have seen a tremendous progress in the development of shock-capturing schemes for nonlinear systems of conservation laws. Among others, we refer to the books [9, 10, 11] (see also the lecture notes [12]) for a concise introduction to these schemes.

Unfortunately, shock-capturing schemes have so far seldom been employed to sedimentation problems. This may in part be due to the fact that mathematical problems related to the analysis of the systems of equations arising from the kinematic approach are far from being well understood. On the other hand, we believe that researchers, for example in chemical engineering, assume the difficulties associated with the presence of shocks to be much greater than they actually are, and instead of solving the conservation equations, they construct solutions of settling problems, e.g., by pre-assuming that the suspension forms a finite number of zones in which the settling velocities of each particle species are constant. A typical view seems to be that expressed by Stamatakis and Tien [13, p. 115]:

> *The particle concentration profiles, in principle, can be found from the solution of the conservation equations of particles of the various types, applying appropriate initial and boundary conditions. The numerical effort involved in solving conservation equations is often excessive (with the main difficulty being the need of adequately taking care of the moving-boundary nature of the suspension/sediment interface). Therefore, it is impractical to examine the dynamics of batch sedimentation using this approach...*

In this paper, we show that batch sedimentation can easily and, to our view, efficiently be examined by a shock-capturing scheme.

Roughly speaking, the shock-capturing schemes may be classified into two categories: central schemes and upwind schemes. The main disadvantage of upwind schemes is the difficulty of solving the Riemann problem exactly or approximately, especially for complex systems of conservation laws. We point out that the (exact or approximate) solution of the Riemann problem for the system of conservation laws that we study in this paper is not known at the moment.

For this reason, we have turned our attention to central schemes. In the 1990s, this class of schemes have received a considerable amount (of renewed) interest, following Nessyahu and Tadmor [14] and their the introduction of the second order sequel to the Lax-Friedrich scheme. We refer to the lecture notes by Tadmor [12] for a general introduction to central schemes and list of relevant references.

The second order central schemes can be viewed as a direct extension of the first order Lax-Friedrich central scheme, which is known to be robust but at same time suffers from excessive dissipation. To resolve this latter problem, the second order central schemes is based on reconstructing, in each time step, a (MUSCL type) piecewise linear interpolant from the cell averages computed in the previous time step. The interpolant is exactly evolved in time and then projected onto its staggered averages, resulting in the staggered cell averages for the next time step. To guarantee the non-oscillatory behaviour of the scheme, the reconstruction uses nonlinear limiters. Unlike upwind schemes, central schemes avoid approximate Riemann solvers, projections along characteristic directions, and the splitting of the flux vector in upwind and downwind directions. This should in principle make this scheme a good candidate for solving complex systems of conservation laws such as the system that we consider in this paper.

In this paper, we shall not use the original central scheme [14] but rather a modified (non-staggered) version introduced recently by Kurganov and Tadmor in [15]. This modified central scheme has a smaller numerical viscosity and is better suited for near steady-state calculations which are of interest in the simulation of sedimentation processes. We refer to Section 3 for further details.

The rest of this paper is organized as follows: in Section 2, we recall the kinematic model of settling of polydisperse ideal suspensions, consider two different constitutive approaches for the slip velocity for each solid species, and derive the respective governing systems of equations. In Section 3 the central schemes are described in detail. In Section 4 one of these schemes is applied to two different test cases: first, we consider the settling of a bidisperse suspension of large and small spheres where the parameters are chosen in such a way that our numerical results can be compared with experimental and theoretical results by Schneider et al. [16]. Second, we consider a three-dimensional particle-scale simulation of the settling of a different bidisperse suspension. In the second case, averaging over each horizontal cross section of the hypothetical settling columns yields concentration profiles for each species that depend only on height, which we compare with the numerical solution of the kinematic model with appropriately chosen parameters. Conclusions that can be drawn from this study are summarized in Section 5.

2. Kinematic model of sedimentation of polydisperse suspensions

For simplicity, we restrict ourselves to an ideal suspension of a fluid with spherical particles of N species of different radii $r_1 > r_2 > \ldots > r_N$ (see [6] for the general case in which the particles are also allowed to have different densities). If we denote by v_i and $\phi_i = \phi_i(x,t)$ the phase velocity and the local volumetric concentration of particle species i, respectively, the mass balances for the solids can be written as

$$\frac{\partial \phi_i}{\partial t} + \frac{\partial f_i}{\partial x} = 0, \quad i = 1, \ldots, N, \tag{1}$$

where $f_i = \phi_i v_i$. These balances lead to a solvable system of N scalar equations if either the solid phase velocities v_i or the solid-fluid relative velocities $u_i = v_i - v_{\mathrm{f}}$, where v_{f} denotes the fluid phase velocity, are given as functions of ϕ_1 to ϕ_N. The former approach is due to Batchelor and Wen [17, 18], while the latter has been advocated by Masliyah [20], see also Concha et al. [7] and Bürger et al. [6].

In both cases, we obtain that the settling of a polydisperse suspension in a column of height L can be described by a system of N conservation laws

$$\frac{\partial \Phi}{\partial t} + \frac{\partial \mathbf{f}(\Phi)}{\partial x} = 0,\ 0 \leq x \leq L,\ t > 0; \quad \mathbf{f}(\Phi) = \big(f_1(\Phi), \ldots, f_N(\Phi)\big)^{\mathrm{T}}, \tag{2}$$

where $\Phi = (\phi_1, \ldots, \phi_N)^{\mathrm{T}}$ denotes the vector of concentration values, together with prescribed initial concentrations

$$\phi_i(x,0) = \phi_i^0(x),\ 0 \leq x \leq L; \quad 0 \leq \phi_1^0(x) + \ldots + \phi_N^0(x) \leq \phi_{\max}, \tag{3}$$

and the zero flux conditions

$$\mathbf{f}|_{x=0} = 0, \quad \mathbf{f}|_{x=L} = 0. \tag{4}$$

It is well known that solutions of equation (2) are discontinuous in general. The propagation speed of a discontinuity in the concentration field ϕ_i is given by the Rankine-Hugoniot condition

$$\sigma_i(\Phi^+, \Phi^-) := \frac{f_i(\Phi^+) - f_i(\Phi^-)}{\phi_i^+ - \phi_i^-}, \quad i = 1, \ldots, N, \tag{5}$$

where Φ^+, ϕ^+, Φ^- and ϕ^- denote the approximate limits of Φ and ϕ from above and from below at the discontinuity, respectively. This condition can readily be derived from the differential equation (2).

2.1. Batchelor's equation

Batchelor derived that in a dilute suspension, the phase velocity of spheres of species i is given by the expression

$$v_i = v_i(\Phi) = u_{\infty i}\left(1 + \sum_{j=1}^{N} S_{ij}\phi_j\right), \tag{6}$$

where $u_{\infty i}$ denotes the Stokes settling velocity of a single particle of radius r_i in pure fluid of density ϱ_{f} and dynamic viscosity μ_{f},

$$u_{\infty i} = -\frac{2\Delta\varrho g r_i^2}{9\mu_{\mathrm{f}}}, \quad i = 1,\dots,N; \quad \Delta\varrho = \varrho_{\mathrm{s}} - \varrho_{\mathrm{f}}, \tag{7}$$

and the coefficients

$$S_{ij} = -3.52 - 1.04\frac{r_j}{r_i} - 1.03\frac{r_j^2}{r_i^2}, \quad i,j = 1,\dots,N$$

are given by a fit to data from Batchelor and Wen [18], which in turn represent numerical evaluations of integrals derived [17], i.e., the coefficients S_{ij} are deduced from first principles.

In order to achieve that $v_i = 0$ when the cumulative solids concentration $\phi := \phi_1 + \ldots + \phi_N$ attains a maximum value $\phi_{\max}$, we replace Batchelor's equation (6) by the expression (see [19])

$$v_i = u_{\infty i} \exp\left(\sum_{j=1}^{N} S_{ij}\phi_j + 2\frac{\phi}{\phi_{\max}}\right)\left(1 - \frac{\phi}{\phi_{\max}}\right)^2, \tag{8}$$

which vanishes for $\phi = \phi_{\max}$ and has the same partial derivatives for $\phi_i = 0$ as (6). Defining the parameters

$$\mu = -\frac{2\Delta\varrho g r_1^2}{9\mu_{\mathrm{f}}}; \ \delta_i = \frac{r_i^2}{r_1^2}, \quad i = 1,\dots,N, \tag{9}$$

we obtain here

$$f_i(\Phi) = f_i^{\mathrm{B}}(\Phi) = \mu\delta_i\phi_i \exp\left(\sum_{j=1}^{N} S_{ij}\phi_j + 2\frac{\phi}{\phi_{\max}}\right)\left(1 - \frac{\phi}{\phi_{\max}}\right)^2. \tag{10}$$

2.2. Masliyah's approach

While formula (6) is based on a postulate for each solids species phase velocity, the following approach essentially involves constitutive equations for the solid-fluid relative velocities $v_i - v_{\mathrm{f}}$, where v_{f} denotes the phase velocity of the fluid.

For batch sedimentation in a closed column, the volume average velocity $q := (1-\phi)v_{\mathrm{f}} + \phi_1 v_1 + \ldots + \phi_N v_N$ vanishes, which can be seen easily by summing equation Eq. (1) over $i = 1,\dots,N$ and by taking into account the continuity equation of the fluid,

$$\frac{\partial\phi}{\partial t} - \frac{\partial}{\partial x}\big((1-\phi)v_{\mathrm{f}}\big) = 0,$$

and that $q = 0$ at $x = 0$. In terms of the relative velocities $u_i := v_i - v_{\mathrm{f}}$, $i = 1,\dots,N$, we can rewrite $q = 0$ as $v_{\mathrm{f}} = -(\phi_1 u_1 + \ldots + \phi_N u_N)$. Noting that $f_i = \phi_i(u_i + v_{\mathrm{f}})$, we obtain

$$f_i = f_i(\Phi) = \phi_i\big(u_i - (\phi_1 u_1 + \ldots + \phi_N u_N)\big).$$

For each species, Masliyah [20] introduced a constitutive equation of the type

$$u_i = \tilde{u}_{\infty i} V(\phi), \tag{11}$$

where $\tilde{u}_{\infty i}$ denotes the Stokes settling velocity of a single particle of species i with respect to a fluid of density $\varrho(\phi) = \phi \varrho_{\mathrm{s}} + (1-\phi)\varrho_{\mathrm{f}}$, i.e.,

$$\tilde{u}_{\infty i} = -\frac{2(\varrho_{\mathrm{s}} - \varrho(\phi)) g r_i^2}{9\mu_{\mathrm{f}}} = -\frac{2(1-\phi)\Delta\varrho g r_i^2}{9\mu_{\mathrm{f}}}, \quad i = 1, \ldots, N, \tag{12}$$

and where $V(\phi)$ can be chosen as one of the hindered settling functions known in the monodisperse case, for example as the well-known Richardson and Zaki [21] formula

$$V(\phi) = V^{\mathrm{RZ}}(\phi) = (1-\phi)^n, \quad n > 1,\ 0 \le \phi \le \phi_{\max}. \tag{13}$$

With the parameters μ and δ_i from (9), we finally obtain

$$f_i(\Phi) = f_i^{\mathrm{M}}(\Phi) = \mu(1-\phi)V(\phi)\biggl(\phi_i \sum_{j=1}^{N} \delta_j \phi_j - \delta_i \phi_i\biggr). \tag{14}$$

2.3. Special case $N = 2$

In the case of just two particle species, the system of equations (2) reduces to

$$\frac{\partial}{\partial t}\begin{pmatrix}\phi_1\\ \phi_2\end{pmatrix} + \mu \frac{\partial}{\partial x}\left(\left(1 - \frac{\phi}{\phi_{\max}}\right)^2 \exp\left(\frac{2\phi}{\phi_{\max}}\right)\begin{pmatrix}\phi_1 \exp(S_{11}\phi_1 + S_{12}\phi_2)\\ \delta_2\phi_2 \exp(S_{21}\phi_1 + S_{22}\phi_2)\end{pmatrix}\right) = 0 \tag{15}$$

in the case of f_1 and f_2 given by (10) and to

$$\frac{\partial}{\partial t}\begin{pmatrix}\phi_1\\ \phi_2\end{pmatrix} + \mu \frac{\partial}{\partial x}\left(V(\phi)(1-\phi)\begin{pmatrix}\delta_2\phi_1\phi_2 - \phi_1(1-\phi_1)\\ \phi_1\phi_2 - \delta_2(1-\phi_2)\end{pmatrix}\right) = 0 \tag{16}$$

for f_1 and f_2 given by (14).

3. Second order central schemes

We shall solve the system of conservation laws (2) by a second order shock-capturing scheme introduced first by Nessyahu and Tadmor [14] and later modified by Kurganov and Tadmor [15]. It is the modified version of the scheme that we use here. To make this paper relatively self-contained, we shall state as well as briefly *derive* this scheme below, starting with the original scheme [14], and then we proceed by explaining the modifications needed to obtain the scheme in [15]. The reader may therefore consider this section as a short introduction (primer) to central schemes. We refer to [14, 15] and the lecture notes by Tadmor [12] for a more complete discussion of central schemes.

To approximate the solution Φ of (2), we introduce a mesh in the (x,t)-plane where the spatial grid points are denoted by x_j and the time levels by t_n. We denote the length of the space and time steps by Δx and Δt, respectively, i.e., $x_j = j\Delta x$ and $t_n = n\Delta t$. We choose integers $\mathcal{J}$ and $\mathcal{N}$ such that $\mathcal{J}\Delta x = L$ and $\mathcal{N}\Delta t = T$. Moreover, we let $\lambda = \Delta t/\Delta x$. We shall always assume that Δx and Δt are related through an appropriate CFL condition [14, 15].

In what follows, we derive briefly the central scheme. In doing so, we do not take into account the boundary conditions in (4), which need special care. The boundary scheme will be described in detail towards the end of this section.

At time level t_n, given the cell averages $\{\bar{\Phi}_j^n = (\bar{\phi}_{1,j}^n, \dots, \bar{\phi}_{N,j}^n)^{\mathrm{T}}\}$, we introduce a piecewise linear reconstruction $\Phi(x,t_n)$,

$$\Phi(x,t_n) = \sum_j \Big(\bar{\Phi}_j^n + \frac{1}{\Delta x}\Phi_j'(x - x_j)\Big)\chi_{\left[x_{j-1/2},\, x_{j+1/2}\right]}(x), \tag{17}$$

where $\Phi_j' = (\phi_{1,j}', \dots, \phi_{N,j}')^{\mathrm{T}}$ is the slope vector defined by

$$\phi_{\ell,j}' = \mathrm{MM}\Big(\theta\big[\bar{\phi}_{\ell,j}^n - \bar{\phi}_{\ell,j-1}^n\big],\, \frac{1}{2}\big[\bar{\phi}_{\ell,j+1}^n - \bar{\phi}_{\ell,j-1}^n\big],\, \theta\big[\bar{\phi}_{\ell,j+1}^n - \bar{\phi}_{\ell,j}^n\big]\Big), \tag{18}$$

for $\ell = 1, \dots, N$ and $\theta \in [0,2]$. Here, $\mathrm{MM}(a,b,c)$ is the minmod function which equals $\min(a,b,c)$ if $a,b,c > 0$, $\max(a,b,c)$ if $a,b,c < 0$, and zero otherwise. In particular, this choice of slope vector satisfies (see [14])

$$\frac{1}{\Delta x}\Phi_j' = \frac{\partial}{\partial x}\Phi(x = x_j, t_n) + \mathcal{O}(\Delta x),$$

which ensures second order accuracy wherever the components of $\mathbf{\Phi}$ are smooth. In addition, this choice ensures that the approximation is non-oscillatory.

Now integrating (2) over the space-time volume $[x_j, x_{j+1}] \times [t_n, t_{n+1}]$ yields the following exact equation for the cell averages $\{\bar{\Phi}_{j+1/2}^{n+1}\}$:

$$\begin{aligned}
\bar{\Phi}_{j+1/2}^{n+1} &:= \frac{1}{\Delta x}\int_{x_j}^{x_{j+1}} \Phi(x,t_n)\,dx \qquad (19)\\
&= \bar{\Phi}_{j+1/2}^n - \frac{1}{\Delta x}\left[\int_{t_n}^{t_{n+1}} \mathbf{f}\big(\Phi(x_{j+1},t)\big)\,dt - \int_{t_n}^{t_{n+1}} \mathbf{f}\big(\Phi(x_{j-1},t)\big)\,dt\right],
\end{aligned}$$

where exact integration of (17) gives

$$\bar{\Phi}_{j+1/2}^n := \frac{1}{\Delta x}\int_{x_j}^{x_{j+1}} \Phi(x,t_n)\,dx = \frac{1}{2}\big(\bar{\Phi}_j^n + \bar{\Phi}_{j+1}^n\big) + \frac{1}{8}\big(\Phi_j' - \Phi_{j+1}'\big).$$

Although the piecewise linear interpolant $\Phi(\cdot,t_n)$ may be discontinuous at the points $\{x_{j+1/2}\}$, the solution $\Phi(\cdot, t \geq t_n)$ remains smooth near each x_j for $t \leq t_{n+1}$ provided the CFL condition $\lambda S_{\max}^n < 1/2$ holds, where $S_{\max}^n$ denotes the maximum propagation speed throughout the domain at time t_n.

Thus the time integrals in (19) only involve smooth integrands and they can be computed within second order accuracy by the mid-point rule:

$$\frac{1}{\Delta x}\int_{t_n}^{t_{n+1}} \mathbf{f}(\Phi(x_j,t))\,dt \approx \lambda \mathbf{f}\big(\Phi(x_j, t_{n+1/2})\big), \tag{20}$$

where the point-values at the half time steps are evaluated by Taylor expansion,

$$\Phi_j^{n+1/2} := \Phi(x_j, t_{n+1/2}) \approx \Phi(x_j, t_n) + \frac{\Delta t}{2}\frac{\partial}{\partial t}\Phi(x_j, t = t_n) = \bar{\Phi}_j^n - \frac{\lambda}{2}\mathbf{f}_j'. \tag{21}$$

Here, the slope vector $\mathbf{f}_j' = (f_{1,j}', \dots, f_{N,j}')^{\mathrm{T}}$ is defined by

$$\begin{aligned} f_{j,\ell}' = \mathrm{MM}\Big(&\theta\big[f_\ell(\bar{\Phi}_j^n) - f_\ell(\bar{\Phi}_{j-1}^n)\big], \\ &\frac{1}{2}\big[f_\ell(\bar{\Phi}_{j+1}^n) - f_\ell(\bar{\Phi}_{j-1}^n)\big], \theta\big[f_\ell(\bar{\Phi}_{j+1}^n) - f_\ell(\bar{\Phi}_j^n)\big]\Big), \end{aligned} \tag{22}$$

for $\ell = 1, \dots, N$ and $\theta \in [0, 2]$. In particular, this choice of slope vector ensures second order accuracy in smooth regions, i.e.,

$$\frac{1}{\Delta x}\mathbf{f}_j' = \frac{\partial}{\partial x}\mathbf{f}(\Phi(x = x_j, t_n)) + \mathcal{O}(\Delta x),$$

and that the numerical approximation is non-oscillatory, see [14].

Summing up, we end up with a scheme that consists of a first order predictor step followed by a second order corrector step:

Predictor step.

$$\Phi_j^{n+1/2} = \bar{\Phi}_j^n - \frac{\lambda}{2}\mathbf{f}_j'. \tag{23}$$

Corrector step.

$$\bar{\Phi}_{j+1/2}^{n+1} = \frac{1}{2}\big(\bar{\Phi}_j^n + \bar{\Phi}_{j+1}^n\big) + \frac{1}{8}\big(\Phi_j' - \Phi_{j+1}'\big) - \lambda\Big[\mathbf{f}\big(\Phi_{j+1}^{n+1/2}\big) - \mathbf{f}\big(\Phi_j^{n+1/2}\big)\Big]. \tag{24}$$

We point out that under a suitable CFL condition (see [14]), the central scheme (23-(24) is TVD (Total Variation Diminishing) for a scalar equation and thus converges to a weak solution. Moreover, it satisfies a cell entropy inequality for a scalar equation with strictly convex flux function and thus converges to the physically correct solution in this case, see [14] for further details.

We note that although the predictor-corrector scheme (23)-(24) uses staggered grid cells (i.e., cells that alternate every other time step), the modified version of the scheme (see below) uses a non-staggered grid.

Note that if we use piecewise constant instead of piecewise linear reconstruction in (17), we recover the staggered version of the Lax-Friedrich scheme. The good resolution of the second order central scheme is because the numerical dissipation is considerably lower than in the Lax-Friedrich scheme, which is due to the use of a second order MUSCL type reconstruction.

The dissipation in the central scheme (23)-(24) is $\mathcal{O}((\Delta x)^4/\Delta t)$. Nevertheless, as seen from this expression for the dissipation, the central scheme does not admit a semi-discrete version, i.e., we cannot send Δt to zero for fixed Δx. Hence the scheme is not appropriate for small time step calculations or steady-state calculations as $t \to \infty$. However, the latter are important in the context of sedimentation processes. In a previous paper [6], we applied the central scheme to the kinematic sedimentation model (2), and indeed it turned out that this scheme yielded diffusive results for the (near) steady-state examples (see [6] for further details).

Next we describe a modification of the central scheme proposed by Kurganov and Tadmor [15] which reduces the dissipation to $\mathcal{O}(\Delta x^3)$ and hence make the scheme better suited for steady-state calculations. In particular, this scheme remains second order accurate independent of $\mathcal{O}(1/\Delta t)$ and letting $\Delta t \to 0$ one obtains even a semi-discrete central scheme. The basic idea behind the modified central scheme is to use more accurate information about the local speed of propagation of the discontinuities.

Assume that we have reconstructed a piecewise linear interpolant (17) from the cell averages $\{\bar{\Phi}_j^n\}$ at time t_n. We then estimate the local propagation speeds $\{a_{j+1/2}^n\}$ at the cell boundaries $\{x_{j+1/2}\}$. To this end, let

$$\begin{aligned}\Phi_{j+1/2}^{+} &:= \Phi(x_{j+1/2}+, t_n) = \bar{\Phi}_{j+1}^n - \Phi'_{j+1}/2,\\ \Phi_{j+1/2}^{-} &:= \Phi(x_{j+1/2}-, t_n) = \bar{\Phi}_{j}^n + \Phi'_{j}/2\end{aligned}$$

be the left and right intermediate values of the interpolant $\Phi(x, t_n)$ at $x = x_{j+1/2}$. We then define the local speed of propagation

$$a_{j+1/2}^n = \max\Big\{\rho\Big(\frac{\partial \mathbf{f}}{\partial \Phi}(\Phi_{j+1/2}^{-})\Big), \rho\Big(\frac{\partial \mathbf{f}}{\partial \Phi}(\Phi_{j+1/2}^{+})\Big)\Big\}, \qquad (25)$$

where $\rho(A) = \max|\mu_i(A)|$ and $\{\mu_i(A)\}$ are the eigenvalues of A.

Although it is possible (and sometimes necessary) to use "approximate eigenvalues" here, we have used in this paper the analytical expressions for the eigenvalues to compute the local speeds $\{a_{j+1/2}^n\}$.

Given the piecewise linear interpolant $\Phi(\cdot, t_n)$ defined in (17) and the local speeds $\{a_{j+1/2}^n\}$, the construction of the cell averages $\{\bar{\Phi}_j^{n+1}\}$ at time t_{n+1} proceeds in two steps:

Step 1. The original central scheme is based on averaging over the (staggered) control volume $[x_j, x_{j+1}]$ of fixed size Δx. Instead, let us integrate over the narrower (and non-uniform) control volume $\big[x_{j+1/2,\mathrm{l}}^n, x_{j+1/2,\mathrm{r}}^n\big] \subset [x_j, x_{j+1}]$, where

$$x_{j+1/2,\mathrm{l}}^n = x_{j+1/2} - a_{j+1/2}^n \Delta t, \qquad x_{j+1/2,\mathrm{r}}^n = x_{j+1/2} + a_{j+1/2}^n \Delta t.$$

For $t \le t_{n+1}$, the solution $\Phi(\cdot, t \ge t_n)$ of (2) with piecewise linear initial data (17) prescribed at $t = t_n$ can be non-smooth only inside the control volume $[x_{j+1/2,\mathrm{l}}^n, x_{j+1/2,\mathrm{r}}^n]$ of width

$$\Delta x_{j+1/2}^n := x_{j+1/2,\mathrm{r}}^n - x_{j+1/2,\mathrm{l}}^n = 2a_{j+1/2}^n \Delta t.$$

As in (19), we proceed with exact evaluation of the new cell averages

$$\{\bar{\Psi}_{j+1/2}^{n+1} = (\bar{\psi}_{1,j+1/2}^{n+1}, \dots, \bar{\psi}_{N,j+1/2}^{n+1})^{\mathrm{T}}\}$$

at t_{n+1}, which yields

$$\begin{aligned}\bar{\Psi}^{n+1}_{j+1/2} &:= \frac{1}{\Delta x^n_{j+1/2}} \int_{x^n_{j+1/2,\mathrm{l}}}^{x^n_{j+1/2,\mathrm{r}}} \Phi(x, t_{n+1})\,dx \\ &= \frac{\bar{\Phi}^n_j + \bar{\Phi}^n_{j+1}}{2} + \frac{1 - a^n_{j+1/2}\lambda}{4}\big(\Phi'_j - \Phi'_{j+1}\big) \\ &\quad - \frac{1}{2a^n_{j+1/2}\Delta t}\left[\int_{t_n}^{t_{n+1}} \mathbf{f}\big(\Phi(x^n_{j+1/2,\mathrm{r}}, t)\big)\,dt - \int_{t_n}^{t_{n+1}} \mathbf{f}\big(\Phi(x^n_{j+1/2,\mathrm{l}}, t)\big)\,dt\right].\end{aligned}$$

As we did in (20), using the mid-point rule to approximate the time integrals enables us to write

$$\begin{aligned}\bar{\Psi}^{n+1}_{j+1/2} = \frac{\bar{\Phi}^n_j + \bar{\Phi}^n_{j+1}}{2} + \frac{1 - a^n_{j+1/2}\lambda}{4}\big(\Phi'_j - \Phi'_{j+1}\big) \\ - \frac{1}{2a^n_{j+1/2}}\Big[\mathbf{f}\big(\Phi^{n+1/2}_{j+1/2,\mathrm{r}}\big) - \mathbf{f}\big(\Phi^{n+1/2}_{j+1/2,\mathrm{l}}\big)\Big],\end{aligned} \tag{26}$$

where the mid-point values are obtained by Taylor expansions (similar to what we did in (21)):

$$\begin{aligned}\Phi^{n+1/2}_{j+1/2,\mathrm{l}} &= \Phi^n_{j+1/2,\mathrm{l}} - \frac{\lambda}{2}\mathbf{f}\big(\Phi^n_{j+1/2,\mathrm{l}}\big)', \\ \Phi^n_{j+1/2,\mathrm{l}} &= \bar{\Phi}^n_j + \Phi'_j\big(1/2 - \lambda a^n_{j+1/2}\big), \\ \Phi^{n+1/2}_{j+1/2,\mathrm{r}} &= \Phi^n_{j+1/2,\mathrm{r}} - \frac{\lambda}{2}\mathbf{f}\big(\Phi^n_{j+1/2,\mathrm{r}}\big)', \\ \Phi^n_{j+1/2,\mathrm{r}} &= \bar{\Phi}^n_{j+1} - \Phi'_{j+1}\big(1/2 - \lambda a^n_{j+1/2}\big),\end{aligned} \tag{27}$$

where the slope vectors $f\big(\Phi^n_{j+1/2,\mathrm{l}}\big)'$, $f\big(\Phi^n_{j+1/2,\mathrm{r}}\big)'$ are defined (with obvious changes) as in (22).

Similarly, let

$$\Delta x^n_j = x^n_{j+1/2,\mathrm{l}} - x^n_{j-1/2,\mathrm{r}} = \Delta x - \Delta t(a^n_{j-1/2} + a^n_{j+1/2})$$

denote the width of the (narrow) interval $[x^n_{j-1/2,\mathrm{r}}, x^n_{j+1/2,\mathrm{l}}]$ around x_j (which is free of neighbouring Riemann fans). As before, integrating exactly and then approximating the resulting (two) time integrals by the mid-point rule, we get the following equation for cell averages $\{\bar{\Psi}^{n+1}_j = (\bar{\psi}^{n+1}_{1,j}, \dots, \bar{\psi}^{n+1}_{N,j})^{\mathrm{T}}\}$:

$$\begin{aligned}\bar{\Psi}^{n+1}_j &:= \frac{1}{\Delta x^n_j}\int_{x^n_{j-1/2,\mathrm{r}}}^{x^n_{j+1/2,\mathrm{l}}} \Phi(x, t_{n+1})\,dx \\ &= \bar{\Phi}^n_j - \frac{\lambda}{2}\big(a^n_{j+1/2} - a^n_{j-1/2}\big)\Phi'_j \\ &\quad - \frac{\lambda}{1 - \lambda\big(a^n_{j-1/2} + a^n_{j+1/2}\big)}\Big[\mathbf{f}\big(\Phi^{n+1/2}_{j+1/2,\mathrm{l}}\big) - \mathbf{f}\big(\Phi^{n+1/2}_{j-1/2,\mathrm{r}}\big)\Big],\end{aligned} \tag{28}$$

where $\Phi^{n+1/2}_{j+1/2,\mathrm{l}}$ and $\Phi^{n+1/2}_{j-1/2,\mathrm{r}}$ are defined in (27).

Step 2. In the second (and final) step, we convert the non-uniform cell averages $\{\bar{\Psi}_j^{n+1}\}$, $\{\bar{\Psi}_{j+1/2}^n\}$ into cell averages over the non-staggered grid cells $\{[x_{j-1/2}, x_{j+1/2}]\}$. To this end, we consider a piecewise linear reconstruction over the non-uniform grid cells at time t_{n+1} and then we project its averages onto the original grid. The required piecewise linear reconstruction takes the form

$$\begin{aligned}\Psi(x,t_{n+1}) \;=\; & \sum_j \Big(\bar{\Psi}_{j+1/2}^{n+1} + \Psi'_{j+1/2}(x - x_{j+1/2})\Big)\chi_{\left[x^n_{j+1/2,\mathrm{l}},\, x^n_{j+1/2,\mathrm{r}}\right]}(x) \\ & + \sum_j \bar{\Psi}_j^{n+1} \chi_{\left[x^n_{j-1/2,\mathrm{r}},\, x^n_{j+1/2,\mathrm{l}}\right]}(x),\end{aligned} \tag{29}$$

where the discrete derivative $\Psi'_{j+1/2} = (\psi'_{1,j+1/2}, \ldots, \psi'_{N,j+1/2})^{\mathrm{T}}$ is defined by

$$\begin{aligned}\psi'_{\ell,j+1/2} = \frac{2}{\Delta x}\mathrm{MM}\Bigg(&\theta\frac{\bar{\psi}^{n+1}_{\ell,j+1/2} - \bar{\psi}^{n+1}_{\ell,j}}{1 + \lambda\big(a^n_{j+1/2} - a^n_{j-1/2}\big)}, \\ &\frac{\bar{\psi}^{n+1}_{\ell,j+1} - \bar{\psi}^{n+1}_{\ell,j}}{2 + \lambda\big(2a^n_{j+1/2} - a^n_{j-1/2} - a^n_{j+3/2}\big)}, \\ &\theta\frac{\bar{\psi}^{n+1}_{\ell,j+1} - \bar{\psi}^{n+1}_{\ell,j+1/2}}{1 + \lambda\big(a^n_{j+1/2} - a^n_{j+3/2}\big)}\Bigg), \quad \theta \in [0,2],\end{aligned} \tag{30}$$

for $\ell = 1, \ldots, N$. Here, one should keep in mind that $\bar{\Psi}_j^{n+1}$ and $\bar{\Psi}_{j+1/2}^{n+1}$ are averages over grid cells centered around

$$x = \frac{1}{2}(x^n_{j-1/2,\mathrm{r}} + x^n_{j+1/2,\mathrm{l}}) = \frac{1}{2}(x_{j-1/2} + x_{j+1/2}) + \frac{\Delta t}{2}\big(a^n_{j-1/2} - a^n_{j+1/2}\big)$$

and $x = x_{j+1/2}$, respectively.

Note that simple averaging over $[x_{j-1/2}, x_{j+1/2}]$ reduces the accuracy of the (resulting) scheme to first order. It is therefore necessary to use the piecewise linear reconstruction (29) in order to not loose the second order accuracy in the process of converting the non-uniform cell averages $\{\bar{\Psi}_j^{n+1}\}$, $\{\bar{\Psi}_{j+1/2}^n\}$ into cell averages over the non-staggered cells $\{[x_{j-1/2}, x_{j+1/2}]\}$. Moreover, note that it is not necessary to reconstruct on the intervals $\{[x^n_{j-1/2,\mathrm{r}},\, x^n_{j+1/2,\mathrm{l}}]\}$ since the solution is smooth there.

Finally, the cell averages $\{\bar{\Phi}_j^{n+1}\}$ are obtained by averaging (29):

$$\begin{aligned}\bar{\Phi}_j^{n+1} \;:=\; & \frac{1}{\Delta x}\int_{x_{j-1/2}}^{x_{j+1/2}} \Psi(x,t_{n+1})\,dx \\ =\; & \lambda a^n_{j-1/2}\bar{\Psi}^{n+1}_{j-1/2} + \lambda a^n_{j+1/2}\bar{\Psi}^{n+1}_{j+1/2} + \big[1 - \lambda(a^n_{j-1/2} + a^n_{j+1/2})\big]\bar{\Psi}_j^{n+1} \\ & + \frac{\Delta x}{2}\big[\big(\lambda a^n_{j-1/2}\big)^2\Psi'_{j-1/2} - \big(\lambda a^n_{j+1/2}\big)^2\Psi'_{j+1/2}\big],\end{aligned} \tag{31}$$

where $\bar{\Psi}^{n+1}_{j-1/2}$, $\bar{\Psi}_j^{n+1}$, $\bar{\Psi}^{n+1}_{j+1/2}$ are defined in (26) and (28).

It is the scheme (31) that is used in the numerical examples presented in this paper, while the original central scheme (23)-(24) has been applied to (2) in our previous paper [6]. For a discussion of the mathematical properties of the modified central scheme (31), we refer to [15] (see also [14]).

Before we can apply (31), it remains to describe the treatment of the boundary conditions in (4). We apply the interior scheme (31) when the index j runs over $3/2, 5/2, \ldots, \mathcal{J}-3/2$. Next we present the boundary scheme, i.e., the updating formulas for $j = 1/2, \mathcal{J}-1/2$. To this end, we note that the central scheme (31) can be written on conservative form:

$$\bar{\Phi}_j^{n+1} = \bar{\Phi}_j^n - \lambda\Big[\mathcal{F}_{j+1/2}^n - \mathcal{F}_{j-1/2}^n\Big], \tag{32}$$

where the numerical flux $\mathcal{F}_{j+1/2}^n$ is defined as

$$\begin{aligned}\mathcal{F}_{j+1/2}^n = {} & \frac{1}{2}\big(\mathbf{f}\big(\Phi_{j+1/2,\mathrm{r}}^{n+1/2}\big) + \mathbf{f}\big(\Phi_{j+1/2,\mathrm{l}}^{n+1/2}\big)\big) - \frac{1}{2}a_{j+1/2}^n\big(\bar{\Phi}_{j+1}^n - \bar{\Phi}_j^n\big) \\ & + \frac{1}{4}a_{j+1/2}^n\big(1 - \lambda a_{j+1/2}^n\big)\big(\Phi_j' + \Phi_{j+1}'\big) + \frac{\Delta x}{2}\lambda\big(a_{j+1/2}^n\big)^2\Psi_{j+1/2}',\end{aligned}$$

where $\Phi_{j+1/2,\mathrm{l}}^{n+1/2}$, $\Phi_{j+1/2,\mathrm{r}}^{n+1/2}$ are defined in (27); $a_{j+1/2}^n$ is defined in (25); Φ_j', Φ_{j+1}' are defined in (18); and $\Psi_{j+1/2}'$ is defined in (30).

Roughly speaking, the boundary treatment consists in setting the numerical fluxes to zero at the boundaries according to the boundary conditions (4). For $j = 1/2$ and $j = \mathcal{J}-1/2$, (32) then reads

$$\bar{\Phi}_{1/2}^{n+1} = \bar{\Phi}_{1/2}^n - \lambda\mathcal{F}_1^n, \qquad \bar{\Phi}_{\mathcal{J}-1/2}^{n+1} = \bar{\Phi}_{\mathcal{J}-1/2}^n + \lambda\mathcal{F}_{\mathcal{J}-1}^n.$$

To compute $\mathcal{F}_1^n$ and $\mathcal{F}_{\mathcal{J}-1}^n$, we set respectively $\Phi_{1/2}' = \Psi_1' = 0$ and $\Phi_{\mathcal{J}-1/2}' = \Psi_{\mathcal{J}-1}' = 0$.

In the numerical calculations shown later, we used 0.6 as the CFL number and 400 grid cells for the spatial discretization. Moreover, in calculating the numerical derivatives we used $\theta = 2$.

4. Numerical examples

We consider two different cases of settling of a homogeneous suspension with solid particles of two different sizes. It is customary to use the radius of the largest particles as a length unit, while the time unit is the Stokes time t_{St}, that is the time a particle of the species having the largest (in absolute value) Stokes settling velocity needs to travel its own radius, i.e.,

$$t_{\mathrm{St}} = \frac{r_1}{u_{\infty 1}} = \frac{9\mu_{\mathrm{f}}}{2\Delta\varrho g r_1}.$$

A dimensionless constant characterizing the hindrance effect exerted by the viscosity of the fluid is the sedimentation Reynolds number

$$\mathrm{Re} = \frac{u_{\infty N} r_N}{\nu_{\mathrm{f}}} = \frac{2\Delta\varrho\varrho_{\mathrm{f}} g r_N^3}{9\mu_{\mathrm{f}}^2}, \tag{33}$$

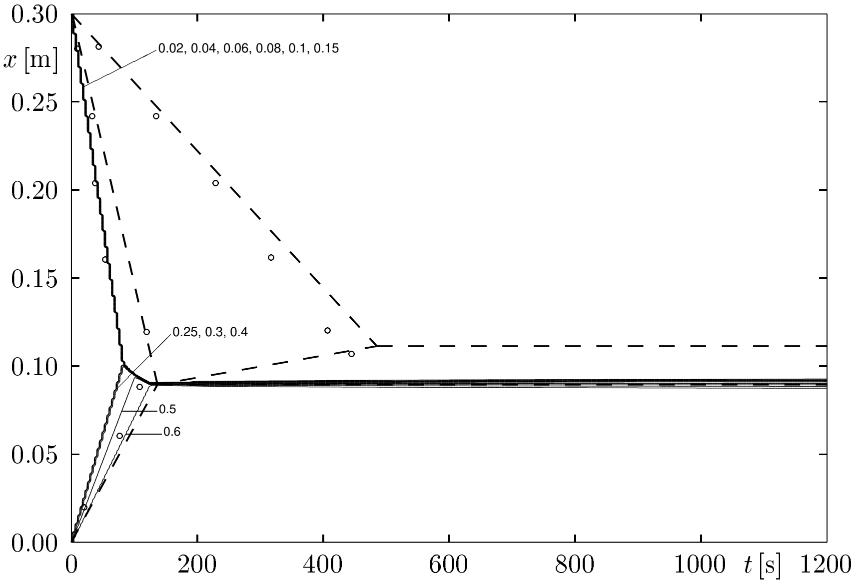

Figure 1. Numerical solution of the kinematic model of settling of a bidisperse suspension: iso-concentration lines of the larger particles, corresponding to concentrations 0.02, 0.04, 0.06, 0.08, 0.1, 0.15, 0.25, 0.3, 0.4, 0.5, 0.6. The circles and dashed lines correspond to experimental measurements of interfaces and constructed shock lines due to Schneider et al. [16].

where ν_{f} is the kinematic viscosity of the fluid.

4.1. Comparison with results by Schneider et al. [16]

Schneider et al. [16] report a settling experiment with glass spheres of density $\varrho_{\mathrm{s}} = 2790\,[\mathrm{kg/m^3}]$ and radii $r_1 = 0.248\,[\mathrm{mm}]$, and $r_2 = 0.0625\,[\mathrm{mm}]$. The remaining parameters are $\varrho_{\mathrm{f}} = 1208\,[\mathrm{kg/m^3}]$, $\mu_{\mathrm{f}} = 0.02416\,[\mathrm{Pas}]$, and $L = 0.3\,[\mathrm{m}]$, i.e., we have $t_{\mathrm{St}} = 0.0173\,[\mathrm{s}]$, $\mu = 0.0143\,[\mathrm{m/s}]$, $\delta_2 = 15.745$, and $\mathrm{Re} = 1.74 \times 10^{-3}$. Following Schneider et al. [16], we use Masliyah's approach with the Richardson-Zaki drag law (13) with $n = 2.7$ and cut this function at $\phi_{\max} = 0.68$ as in [7]. The initial concentrations are $\phi_1^0 = 0.2$ and $\phi_2^0 = 0.05$. Figures 1 and 2 show the simulated iso-concentration lines for the larger and the smaller spheres, respectively, together with the experimental measurements of interface locations and shock lines (dashed lines) computed by Schneider et al. [16], while Figure 3 displays concentration profiles of both species at three selected times.

The construction procedure for the shock lines used by Schneider et al. [16] is similar to that proposed by Greenspan and Ungarish [22] and exploits the Rankine-Hugoniot jump condition (5): if one assumes that an initially homogeneous N-disperse suspension settles in such a way that the bulk suspension is separated from the supernatant liquid by $(N-1)$ zones where the concentration is constant, and that the sediment assumes the maximum concentration and is separated from the bulk suspension by a single discontinuity, then the $(N-1)N + (N-1) = N^2 - 1$ unknown concentration values and the unknown

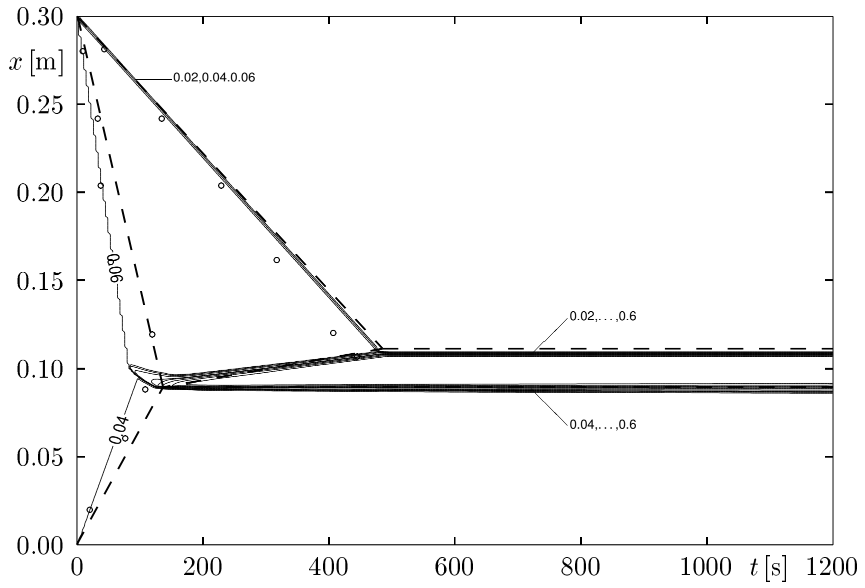

Figure 2. Numerical solution of the kinematic model of settling of a bidisperse suspension: iso-concentration lines of the smaller particles, corresponding to concentrations 0.02, 0.04, 0.06, 0.08, 0.1, 0.15, 0.25, 0.3, 0.4, 0.5, 0.6. The circles and dashed lines correspond to experimental measurements of interfaces and constructed shock lines due to Schneider et al. [16].

propagation speeds of the $N+1$ discontinuities (for small $t>0$) can be calculated from the available $(N+1)N$ scalar Rankine-Hugoniot conditions. This construction procedure is discussed in detail in [6].

Here, we emphasize that this method does not necessarily produce the physically relevant solution, i.e., the entropy weak solution of the sedimentation problem, since it does not include continuous transitions between concentration values by rarefaction waves. In fact, the numerically computed iso-concentration lines shown in Figure 1 clearly show that the sediment forming on the bottom of the column is not separated by a kinematic shock from the bulk suspension at initial concentration. Rather, we observe a rarefaction wave expressed by the spreading of the iso-concentration lines belonging to $\phi_1 = 0.4$, 0.5 and 0.6. This behaviour is also visible in Figure 3 in the profiles of both concentrations near $x = 50\,[\mathrm{mm}]$. Since it is ensured that the numerical scheme approximates the entropy weak solution, we have reason to believe that the rising kinematic shock constructed by Schneider et al. can not be physically correct. Nevertheless, the final composition of the sediment attained after about 500 [s] does coincide with the kinematic shock solution.

We point out that this example has also been considered in our previous paper [6]. However, since we have employed here an improved numerical scheme, the two discontinuities separating the two different final sediment layers and the sediment from the clear supernate appear are less diffusive here. As discussed in Section 3, this due to the fact that the modified central scheme is designed to produce less numerical diffusion for long-time integration (steady-state calculations) than the original central scheme.

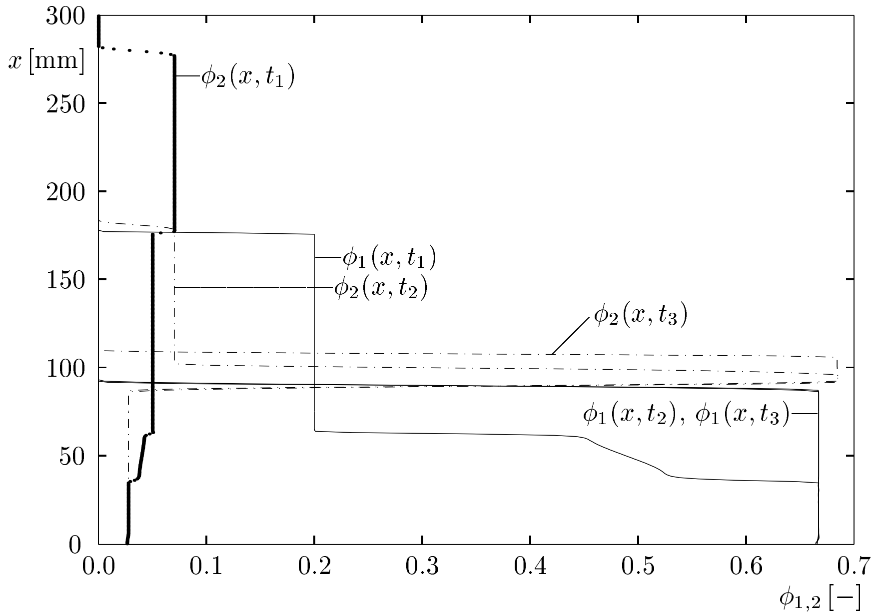

Figure 3. Numerical solution of the kinematic model of settling of a bidisperse suspension: concentration profiles of the larger and of the smaller particles taken at $t_1 = 51.0$ [s], $t_2 = 300.2$ [s], and $t_3 = 599.2$ [s].

4.2. Comparison with a particle-scale simulation

We use a recently developed simulation technique for particle suspensions at low Reynolds numbers [23] to simulate the settling of bidisperse particles in a viscous fluid. This simulation technique resolves the flow on the scale of the particles and has been applied successfully to studies of monodisperse suspensions [23, 24]. In contrast to experiments with real materials, simulations are able to measure not only the total particle concentration but also the local concentrations of each species separately. We are therefore in a position to directly compare the results of the particle-scale simulation with the one-dimensional kinematic model.

4.2.1. *Simulation Technique*

The fluid motion is represented by the incompressible Navier-Stokes equations,

$$\frac{\partial \mathbf{v}_\mathrm{f}}{\partial t} + (\mathbf{v}_\mathrm{f} \cdot \nabla)\mathbf{v}_\mathrm{f} = -\nabla p + \frac{1}{\mathrm{Re}}\nabla^2 \mathbf{v}_\mathrm{f} + \mathbf{f}^l, \tag{34}$$

$$\nabla \cdot \mathbf{v}_\mathrm{f} = 0, \tag{35}$$

where $\mathbf{v}_\mathrm{f}$ is the fluid velocity measured in units of some typical velocity U, $\mathrm{Re} = aU/\nu$ is the particle Reynolds number, a the radius of the spherical particles considered, and ν the dynamic viscosity of the fluid. The pressure p is measured in units of $\varrho_\mathrm{f} U^2$, where ϱ_f is the fluid density. The point force $\mathbf{f}^l$ usually represents body forces like gravity, but local force distributions may be used to model boundary conditions as well (see below). It is convenient to eliminate gravity from the equations since it cancels the induced constant hydrostatic pressure gradient; we then have to add buoyancy when we consider the forces acting on particles.

In order to solve the fluid equations (34) and (35), we use a fixed, regular grid —a staggered marker and cell mesh— for a second order spatial discretization [25]. Moreover, we employ a simple explicit Euler time stepping for the discretization of equation (34) and an implicit determination of the pressure in an operator splitting approach to satisfy the incompressibility constraint at all times. The resulting pressure Poisson equation is solved by multigrid techniques. For more details, see [25, 26].

Physically the suspended particles are moving boundaries in the Navier-Stokes equation which are not easy to represent. We therefore use the volume force term in Eq. (35) to model the interaction between the fluid and the particles.

To this end, we imagine that the physical particles in the fluid are decomposed as follows. We need (i) a rigid particle template endowed with a certain mass m_i^t and moment of inertia I_i^t, which complements (ii) mass and moment of inertia of the volume V_i of liquid covered —but not replaced— by the template. We must require $m_i^t + \varrho_{\mathrm{f}} V_i = m_i$ and $I_i^t + I_f = I_i$, i.e., that template plus liquid volume elements together yield the correct mass m_i and moment of inertia I_i of the physical particle.

In order to achieve the coupling, we distribute reference points j with coordinates $\mathbf{r}_{ij}$ over the particle templates with respect to the center of particle i at $\mathbf{x}_i$. These reference points move due to the translation and rotation of the particle template and follow trajectories $\mathbf{x}_{ij}^r(t)$,

$$\mathbf{x}_{ij}^r(t) = \mathbf{x}_i(t) + \mathbf{O}_i(t)\mathbf{r}_{ij},$$

where $\mathbf{O}_i(t)$ is a matrix describing the orientation of the template. Each reference point is associated with one tracer particle (superscript m) at $\mathbf{x}_{ij}^m$ which is passively advected by the flow field, $\dot{\mathbf{x}}_{ij}^m = \mathbf{v}_{\mathrm{f}}(\mathbf{x}_{ij}^m)$. Whenever the reference point and the tracer are not at the same position, forces shall arise (see below) to make the tracer follow the reference point, i.e., the liquid motion coincides with the particle motion.

Between a tracer and its reference point we introduce a damped spring which gives rise to a force density in the liquid:

$$\mathbf{f}_{ij}^l(\mathbf{x}_{ij}^m) = h^{-d}(-k\boldsymbol{\xi}_{ij} - 2\gamma\dot{\boldsymbol{\xi}}_{ij})\delta(\mathbf{x}_{ij}^m). \tag{36}$$

In this equation, $\boldsymbol{\xi}_{ij} = \mathbf{x}_{ij}^m - \mathbf{x}_{ij}^r$ denotes the distance between the tracer and the reference point, k is the spring constant, γ is the damping constant, $\delta(\mathbf{x})$ the Dirac distribution, and h^d the volume of liquid associated with one marker particle. It should be clear that this force law is largely arbitrary. We have verified that its choice does not have significant influence on the motion of the physical particle as a whole, provided that k is chosen sufficiently large to ensure that ξ_{ij} remains always small and the density of markers is about $1/h^d$ [27].

4.2.2. *Simulation setup*

We consider rigid spheres of radii $r_1 = 1.41$ and $r_2 = 1.0$ in a settling column with quadratic cross-section of size (width $\times$ height $\times$ depth) $= 36 \times 567 \times 36$

with walls at the bottom and top and periodic boundary conditions in the other directions. The densities are $\varrho_{\mathrm{f}} = 1$ for the fluid and $\varrho_{\mathrm{s}} = 2.5$ for the particles, and the gravity constant is $g = 30$. We choose $\nu_{\mathrm{f}} = 10$ so that the Stokes velocities are $u_{\infty 1} = 2$ for the larger and $u_{\infty 2} = 1$ for the smaller particles. Due to the finite size of the container, the single particle settling velocity is less than the stokes velocity [28]. We account for this effect by scaling the parameter μ in Eq. (10) with the appropriate value of 0.85 by substitution of μ with $\mu' = 0.85\mu$.

The Reynolds number is $\mathrm{Re} = 0.1$ and $t_{\mathrm{St}} = 1$. The initial concentrations are $\phi_1^0 = \phi_2^0 = 0.05$. Figures 3 and 4 show the iso-concentration lines for the larger and for the smaller particles, respectively, obtained from the three-dimensional simulation compared to those determined by numerical solution of the one-dimensional kinematic model. In Figures 5 and 6, the corresponding concentration profiles for $t = 100t_{\mathrm{St}}$, $t = 300t_{\mathrm{St}}$, $t = 500t_{\mathrm{St}}$ and $t = 800t_{\mathrm{St}}$ are compared. In the kinematic sedimentation model, we employ the modified Batchelor formula (8). From the given radii, we obtain the coefficients

$$S_{11} = S_{22} = -5.6, \quad S_{12} = -7.05, \quad S_{21} = -4.77.$$

The remaining parameters are $\mu' = 1.7$ and $\delta_2 = 1/2$.

4.2.3. *Discussion of numerical results*

In Figures 4 and 5, we compare the iso-concentration lines calculated by numerical solution of the kinematic one-dimensional model with those obtained from the three-dimensional particle scale simulation, while Figures 6 and 7 show the same result as a selection of concentration profiles. The agreement between the 'kinematic' and the 'particle scale' types of results visible in these figures indicates that the kinematic model describes fairly well the global behaviour of the suspension and predicts correctly the location of fronts.

As a first conclusion, this illustrates that the use of periodic lateral boundary conditions in combination with a global correction of settling velocities in the three-dimensional simulation is the correct way to represent the "bulk" situation, i.e., sedimentation in which all effects are not appreciable. The importance of this observation lies, of course, in the fact that three-dimensional particle scale simulations can be performed only in a column of relatively small (compared to the particle size) cross-sectional area.

The numerical iso-concentration lines always represent shock lines, i.e. concentration discontinuities in this example. Their location agrees well with those of the particle scale approach. This is in particular valid for the interfaces separating the sediment from the supernatant suspension or clear liquid. Moreover, we observe that the kinematic model predicts very accurately the thickness and concentration of the thin layer of the smaller particles forming above the sediment of mixed composition, as visible in Figure 7.

Of course, effects referring to a length scale of particle size such as those described by hydrodynamic diffusion are neglected in the kinematic approach. This becomes apparent in the smearing of sharp interfaces visible in all figures, and in part in concentration fluctuations in zones where the kinematic model predicts constant concentrations.

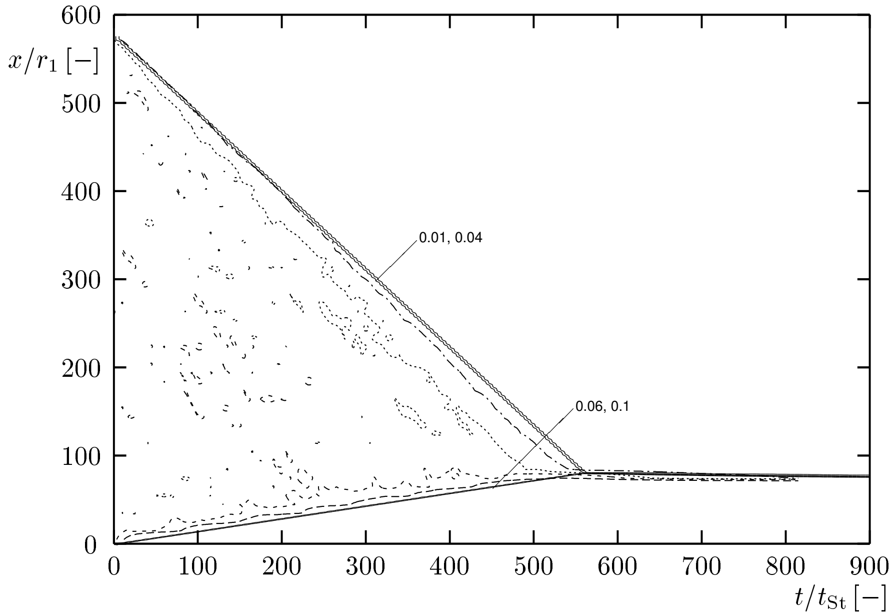

Figure 4. Particle-scale simulation and numerical solution of the kinematic model of the settling of a bidisperse suspension: iso-concentration lines of the larger spheres. The solid lines correspond to the numerical solution and to the annotated concentration values. The long-dashed, short-dashed, dotted and dash-dotted lines have been obtained by particle-scale simulation and correspond to $\phi_1 = 0.1$, $\phi_1 = 0.06$, $\phi_1 = 0.04$, and $\phi_1 = 0.01$, respectively.

It is, however, interesting to note that Figure 7 clearly illustrates that the 'enrichment' of the smaller solid particles between the two downwards propagating shocks visible in the rectangular 'noses' of the concentration profiles for $t = 100t_{\mathrm{St}}$, $t = 300t_{\mathrm{St}}$ and $t = 500t_{\mathrm{St}}$ (corresponding to the area between the two numerical iso-concentration lines $\phi_2 = 0.06$ in Figure 5) is due to kinematic effects, and not to hydrodynamic diffusion. The contrary seems to be true e.g. for the strongly scattered 'particle scale' concentration profile for $t = 100t_{\mathrm{St}}$ in Figure 6.

5. Conclusions

In this paper we have shown that high-resolution shock capturing schemes of central type (i.e., Riemann solver free) can be used as an efficient tool for the numerical solution of the kinematic model of sedimentation of polydisperse suspensions of spheres, although their development had been oriented toward different applications. Their approximation of the physically relevant solution, the entropy solution, produces solutions showing more details compared to "kinematic shock" constructions [16, 22]. Due to their explicit nature, these schemes are fairly easy to implement, and should be applied to additional theoretical and practical problems arising from the theory of sedimentation of polydisperse suspensions. Most notably, it can be hoped that reliable nu-

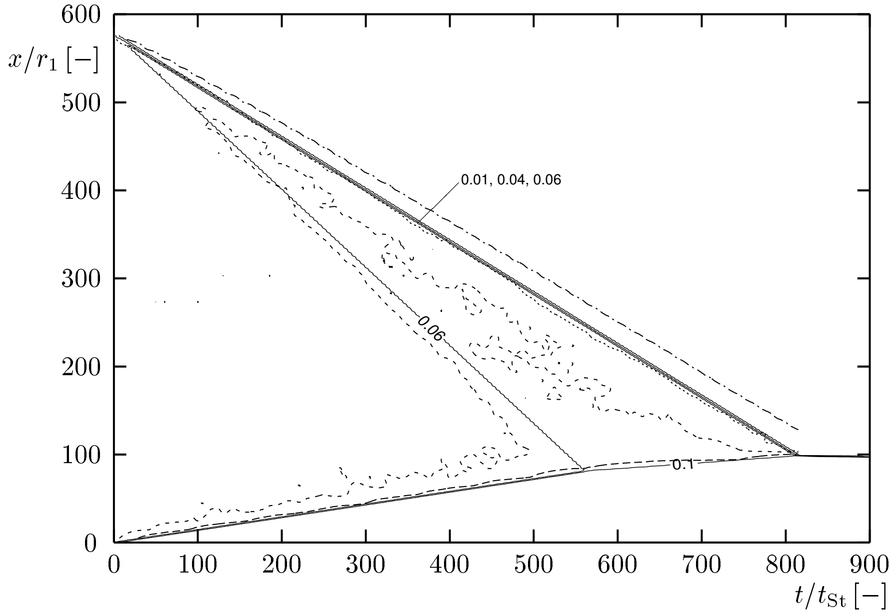

Figure 5. Particle-scale simulation and numerical solution of the kinematic model of the settling of a bidisperse suspension: iso-concentration lines of the smaller spheres. The solid lines correspond to the numerical solution and to the annotated concentration values. The long-dashed, short-dashed, dotted and dash-dotted lines have been obtained by particle-scale simulation and correspond to $\phi_2 = 0.1$, $\phi_2 = 0.06$, $\phi_2 = 0.04$, and $\phi_2 = 0.01$, respectively.

merical solutions will yield additional insights for the analytical determination of the possible modes of sedimentation behaviour of an initially homogeneous polydisperse suspension in a settling column, which is still an open problem in contrast to the relatively simple monodisperse case [1].

It has been found that the predictions of the phenomenological theory of sedimentation of flocculated suspensions, an extension of Kynch's theory [5] for monodisperse systems which includes compression effects and leads to a degenerate parabolic PDE for the local solids concentration, compare quite well with results from settling experiments [29]. However, only few experiments have been performed to validate the kinematical model of sedimentation of polydisperse suspensions, since it is very difficult (if not impossible) even to prepare a 'real' initially homogeneous polydisperse suspension.

The quality of agreement between both types of results discussed in § 4.2.3 demonstrates that comparison with particle-scale simulation is a serious easier alternative to assess the validity of the widely used kinematic models. Of course, a particle scale simulation yields much more details of a flow than the kinematic approach. However, as the preceding brief discussion of 'enrichment' of small particles has shown, the solution of a kinematic model with a reliable, i.e. entropy satisfying shock-capturing scheme may help to interpret results obtained from three-dimensional simulations and to draw additional conclusion from a given simulation, for example which phenomena would persist even if the ratio of particle size and vessel dimensions tend to zero. Therefore we believe that

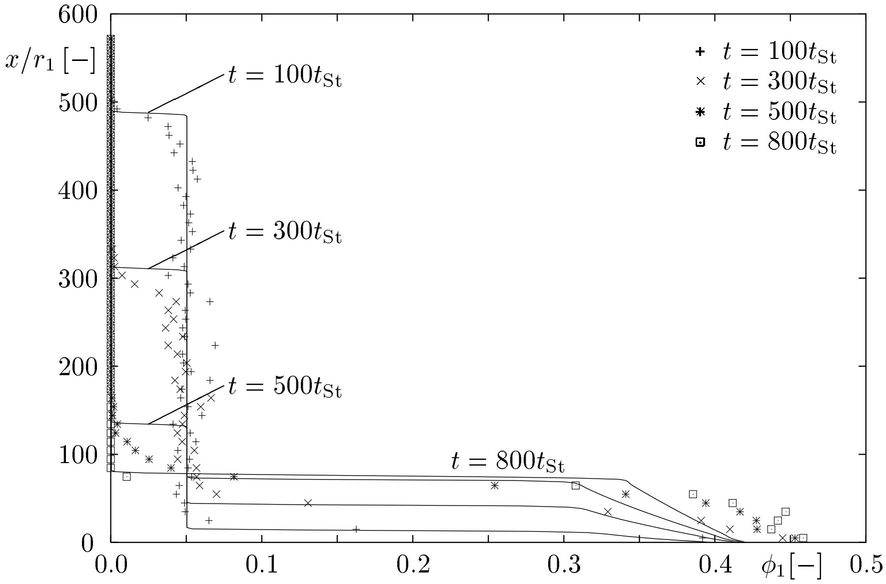

Figure 6. Particle-scale simulation (symbols) and numerical solution of the kinematic model (solid lines) of the settling of a bidisperse suspension: concentration profiles of the larger spheres.

the kinematics approach and its particular numerical discretization outlined here are a valuable tool even in applications where the fully three-dimensional particle scale approach is essential.

Acknowledgements

We acknowledge financial support by the Sonderforschungsbereich 404 at the University of Stuttgart and by the Applied Mathematics in Industrial Flow Problems (AMIF) programme of the European Science Foundation (ESF). We would like thank the Norwegian Research Council for financial support of Kjell Kåre Fjelde and Kenneth Hvistendahl Karlsen through the Strategic Institute Program "Complex Wells".

References

1. M.C. Bustos, F. Concha, R. Bürger and E.M. Tory, *Sedimentation and Thickening.* Dordrecht: Kluwer Academic Publishers (1999) 304pp.
2. G.A. Ekama, J.L. Barnard, F.W. Günthert, P. Krebs, J.A. McCorquodale, D.S. Parker and E.J. Wahlberg, *Secondary Settling Tanks.* London: International Association on Water Quality (1997) 232pp.
3. W.K. Sartory, Three-component analysis of blood sedimentation by the method of characteristics, *Math. Biosci.* 33 (1977) 145–165.
4. P.T. Shannon, E. Stroupe and E.M. Tory, Batch and continuous thickening, *Ind. Engrg. Chem. Fund.* 2 (1963) 203–211.

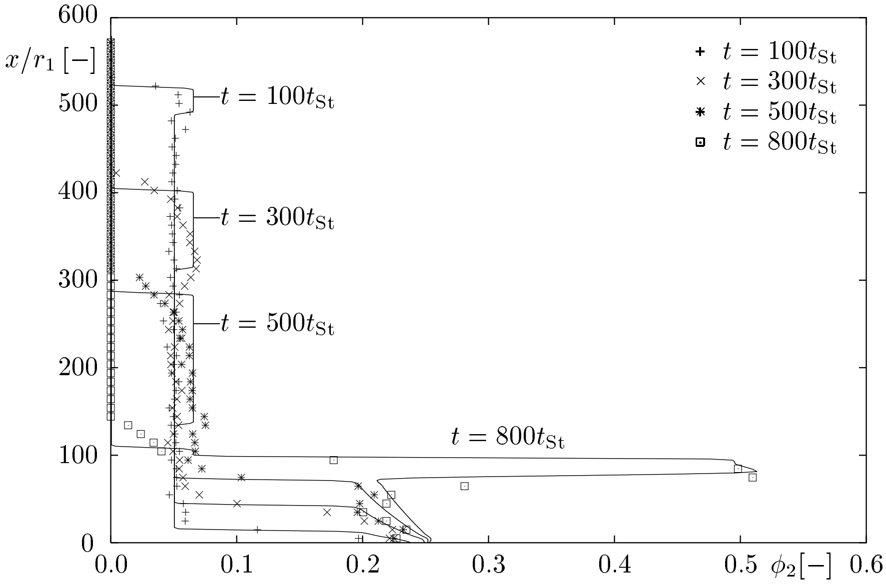

Figure 7. Particle-scale simulation (symbols) and numerical solution of the kinematic model (solid lines) of the settling of a bidisperse suspension: concentration profiles of the smaller spheres.

5. G.J. Kynch, A theory of sedimentation, *Trans. Faraday Soc.* 48 (1952) 166–176.
6. R. Bürger, F. Concha, K.-K. Fjelde and K.H. Karlsen, Numerical simulation of the settling of polydisperse suspensions of spheres. *Powder Technol.*, to appear.
7. F. Concha, C.H. Lee and L.G. Austin, Settling velocities of particulate systems: 8. Batch sedimentation of polydispersed suspensions of spheres, *Int. J. Mineral Process.* 35 (1992) 159–175.
8. Y.T. Shih, D. Gidaspow and D.T. Wasan, Hydrodynamics of sedimentation of multisized particles, *Powder Technol.* 50 (1987) 201–215.
9. E. Godlewski and P.-A. Raviart, *Numerical approximation of hyperbolic systems of conservation laws.* New York: Springer Verlag (1996) 509pp.
10. R. J. LeVeque, *Numerical methods for conservation laws.* Basel: Birkhäuser Verlag, Second Ed., (1992) 214pp.
11. E. F. Toro, *Riemann solvers and numerical methods for fluid dynamics.* Berlin: Springer Verlag (1997) 610pp.
12. E. Tadmor, Approximate solutions of nonlinear conservation laws, in A. Quarteroni (ed.), *Lecture notes in Mathematics 1697, 1997 C.I.M.E. course in Cetraro, Italy, June 1997.* Berlin: Springer Verlag (1998) pp. 1–149.
13. K. Stamatakis and C. Tien, Dynamics of batch sedimentation of polydispersed suspensions, *Powder Technol.* 56 (1988) 105–117.
14. H. Nessyahu and E. Tadmor, Nonoscillatory central differencing for hyperbolic conservation laws, *J. Comput. Phys.* 87 (1990) 408–463.
15. A. Kurganov and E. Tadmor, New high resolution central schemes for nonlinear conservation laws and convection-diffusion equations. Los Angeles: University of California at Los Angeles, UCLA-CAM Report 16 (1999).
16. W. Schneider, G. Anestis and U. Schaflinger, Sediment composition due to settling of particles of different sizes, *Int. J. Multiphase Flow* 11 (1985) 419–423.
17. G.K. Batchelor, Sedimentation in a dilute polydisperse system of interacting spheres. Part1. General theory, *J. Fluid Mech.* 119 (1982) 379–408.

18. G.K. Batchelor and C.S. Wen, Sedimentation in a dilute polydisperse system of interacting spheres. Part 2. Numerical results, *J. Fluid Mech.* 124 (1982) 495–528.
19. K. Höfler and S. Schwarzer, The structure of bidisperse suspensions at low Reynolds numbers, in W.L. Wendland, W. Ehlers, H. Herrmann, C. Miehe, A.-M. Sändig and W. Schiehlen (eds.), *Multifield Problems in Solid and Fluid Mechanics.* Berlin: Springer Verlag, to appear.
20. J.H. Masliyah, Hindered settling in a multiple-species particle system, *Chem. Engrg. Sci.* 34 (1979) 1166–1168.
21. J.F. Richardson and W.N. Zaki, Sedimentation and fluidization I, *Trans. Instn. Chem. Engrs. (London)* 32 (1954) 35–53.
22. H.P. Greenspan and M. Ungarish, On hindered settling of particles of different sizes, *Int. J. Multiphase Flow* 8 (1982) 587–604.
23. K. Höfler and S. Schwarzer, Navier-Stokes simulation with constraint forces: A finite-difference method for particle-laden flows and complex geometries. Submitted to *Phys. Rev. E* (1999).
24. B. Wachmann and S. Schwarzer, Three-dimensional massively parallel computing of suspensions, *Int. J. Mod. Phys. C* 9 (1998) 759–775.
25. R. Peyret and T. D. Taylor, *Computational Methods for Fluid Flow.* New York: Springer Verlag (1983).
26. W. Kalthoff, S. Schwarzer and H. Herrmann, Algorithm for the simulation of particle suspensions with inertia effects, *Phys. Rev. E* 56 (1997) 2234–2242.
27. K. Höfler, *Räumliche Simulation von Zweiphasenflüssen.* Stuttgart: Diploma Thesis, Institute for Computer Applications I, University of Stuttgart (1997) 82pp.
28. H. Hasimoto, On the periodic fundamental solutions of the Stokes equations and their application to viscous flow past a cubic array of spheres, *J. Fluid Mech.* 5 (1959) 317–328.
29. R. Bürger, F. Concha and F.M. Tiller, Applications of the phenomenological theory to several published experimental cases of sedimentation processes, *Separ. Purif. Technol.*, to appear in a special issue.